Lowermost mantle anisotropy beneath the northwestern Pacific: Evidence from PcS, ScS, SKS, and SKKS phases

Xiaobo He and Maureen D. Long

Department of Geology and Geophysics, Yale University, 210 Whitney Avenue, New Haven, Connecticut 06511, USA (xiaobo.he@yale.edu)

[1] In this study, we utilize data from broadband seismic stations of the Japanese F-net network to investigate anisotropic structure in the lowermost mantle beneath the northwestern Pacific. The comparison of shear wave splitting from phases that have similar paths in the upper mantle but different paths in the lowermost mantle, such as PcS/ScS or SKS/SKKS, can yield constraints on anisotropy in the D″ region. We measured splitting for SKS, SKKS, PcS, and ScS phases at F-net stations and compared the measured splitting parameters to previously published estimates of upper mantle anisotropy beneath the region. We observed many examples of discrepant SKS/SKKS splitting and splitting of ScS, PcS, SKS, and SKKS phases that does not agree well with the known upper mantle anisotropy beneath individual stations. The most likely explanation for these discrepancies is a contribution to splitting from anisotropy in the lowermost mantle. In particular, for SKS/SKKS phases that sample the lowermost mantle just to the south and east of the Kamchatka peninsula, we observed generally N-S fast directions with delay times between 0.5 and 1.5 s. These data suggest the presence of a fairly large, coherent region of deformation in the lowermost mantle beneath the northwestern Pacific. Our preferred model for these observations is that solid-state flow at the base of the mantle induces a lattice-preferred orientation of lowermost mantle minerals, generating a seismically anisotropic fabric.

1. Introduction

[2] The lowermost ∼200–300 km of the mantle, known as the D″ layer, represents the most important thermo-chemical boundary region in the Earth's interior, and its seismological properties are striking. In contrast to the overlying lower mantle, D″ is a region of strong lateral heterogeneity in velocity structure [e.g., *Houser et al.*, 2008], which has been interpreted as evidence for heterogeneity in both thermal and chemical structure [e.g., *Trampert et al.*, 2004]. Seismologists have detected a seismic discontinuity for both P and S waves with a change in vertical velocity gradient at the top of the D″ layer

[e.g., *Wysession et al.*, 1998; *Lay et al.*, 2004; *Lay and Garnero*, 2007], although the presence, depth, sharpness, and other characteristics of the discontinuity vary laterally [e.g., *Garnero and McNamara*, 2008] and a double discontinuity has been suggested in some regions [e.g., *Hernlund et al.*, 2005; *van der Hilst et al.*, 2007]. It has been suggested that the D″ discontinuity is caused by a phase transformation from magnesium silicate perovskite to post-perovskite [e.g., *Murakami et al.*, 2004]. A thin (∼10 km) layer of ultra-low velocity is present at the base of the mantle in several local regions [e.g., *Thorne and Garnero*, 2004; *Garnero and Thorne*, 2007], which could indicate the presence of partial melt and/or chemically distinct material [e.g., *McNamara et al.*, 2010].

[3] D″ is also distinguished from the overlying lower mantle by the presence of seismic anisotropy. To first order, the lower mantle is thought to be generally isotropic [e.g., *Meade et al.*, 1995; *Visser et al.*, 2008], but there is growing observational evidence for significant anisotropy in D″ [e.g., *Kendall and Silver*, 1996; *Lay et al.*, 1998; *Garnero et al.*, 2004; *Panning and Romanowicz*, 2004; *Wookey et al.*, 2005; *Wang and Wen*, 2007; *Wookey and Kendall*, 2008; *Long*, 2009; *Nowacki et al.*, 2010]. Because seismic anisotropy in the Earth's mantle is a consequence of deformation, observations of anisotropy in the D″ region can potentially be used to map patterns of flow at the base of the mantle, which would yield powerful insight into lower mantle dynamics. However, the interpretation of D″ anisotropy measurements remains uncertain, because the cause of lowermost mantle anisotropy is still unknown. One possibility is that anisotropy is due to the lattice-preferred orientation (LPO) of lowermost mantle minerals, perhaps including perovskite [e.g., *Stixrude*, 1998; *Kendall and Silver*, 1998], post-perovskite [e.g., *Tsuchiya et al.*, 2004; *Stackhouse et al.*, 2005; *Wentzcovitch et al.*, 2006], or ferropericlase [e.g., *Karato*, 1998; *Karki et al.*, 1999; *Marquardt et al.*, 2009]. Alternatively, the anisotropy could be produced by the shape-preferred orientation (SPO) of inclusions of downgoing materials from subducted plates or partial melt at the lowermost mantle [e.g, *Kendall and Silver*, 1996, 1998].

[4] Detailed observations of the geometry and strength of anisotropy in different regions of the lowermost mantle may help to discriminate among the various possible mechanisms and eventually pave the way for the interpretation of D″ anisotropy in terms of mantle flow. Most constraints on D″ anisotropy come from observations of the splitting or birefringence of shear waves that have sampled the lowermost mantle. When a shear wave passes through an anisotropic medium, it splits into orthogonally polarized components with different wave speeds and the fast direction (ϕ) and delay time (δt) contain information about the geometry and strength of anisotropy. From an observational point of view, there are several challenges in studying D″ anisotropy. Chief among these is the need to account for the signal of anisotropy in the upper mantle near the receiver (and perhaps near the source) in order to properly isolate the signal from D″. A compelling solution is to find pairs of phases that have the nearly same paths near the source and receiver, but sample different parts of D″; any difference in splitting can then be attributed to anisotropic structure in the deepest mantle. In this way, the differential splitting of phases such as S/ScS [e.g., *Wookey et al.*, 2005; *Nowacki et al.*, 2010] and SKS/SKKS [e.g., *Niu and Perez*, 2004; *Restivo and Helffrich*, 2006; *Long*, 2009] has been used to study anisotropy in the lowermost mantle. In an alternative to this approach, waveforms can be explicitly corrected for the effect of upper mantle anisotropy beneath the receiver before D″-associated splitting is measured, usually using previously published estimates of average SKS splitting [e.g., *Fouch et al.*, 2001; *Rokosky et al.*, 2004; *Ford et al.*, 2006]. However, if there are backazimuthal variations in receiver-side splitting due to complex anisotropy in the upper mantle beneath the station, then applying accurate receiver-side corrections can be difficult and errors in the estimates of lowermost mantle splitting can be introduced.

[5] In this study, we examined the splitting of SKS, SKKS, PcS and ScS phases (Figure 1) measured at stations of the Japanese F-net network to study anisotropy in the lowermost mantle beneath the northwestern Pacific. Although upper mantle anisotropy beneath Japan is complicated, it has been studied in great detail and splitting patterns due to upper mantle anisotropy beneath F-net stations are well known [*Long and van der Hilst*, 2005]. Additionally, the average delay times at F-net stations obtained using the splitting intensity measurement method are generally small, with many $\delta t < 0.5$. We identified high-quality SKS and SKKS arrivals at F-net stations with well-constrained splitting measurements for the same event-station pair; any discrepancies in splitting between the two phases can be attributed to anisotropic structure in the lower mantle, far from the receiver. For PcS and ScS phases, we compared our measured splitting parameters with estimates of splitting due to upper
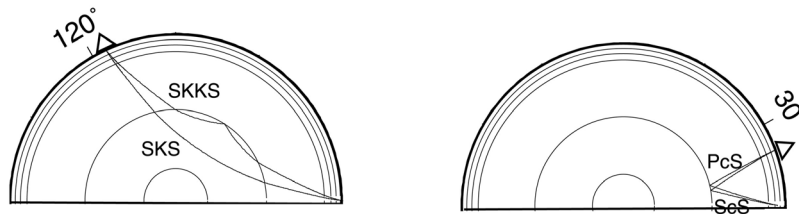
Figure 1. A schematic illustration of raypaths used in this study. (left) SKS/SKKS; (right) ScS/PcS.

mantle anisotropy beneath F-net stations from *Long and van der Hilst* [2005], focusing on stations with relatively simple upper mantle anisotropy. Discrepancies between PcS/ScS splitting and the expected splitting due to upper mantle structure can be attributed to anisotropy in the deepest mantle, with a possible contribution to splitting from source-side anisotropy for ScS phases.

2. Data and Methods

[6] We collected broadband waveform data from stations of the Japanese F-net array (Figure 2), operated by the National Institute for Earth Science

and Disaster Prevention (NIED). For PcS and ScS phases (Figure 1), we selected earthquakes that occurred at depths greater than 300 km; we restricted our analysis to deep events to minimize any contribution to splitting of ScS phases from anisotropy near the source (this is discussed further in section 4.2). Events at epicentral distances less than 25° were selected so that the core-mantle boundary (CMB) bounce points sampled the lowermost mantle beneath the northwestern Pacific, and so the incidence angles in the upper mantle beneath the receivers were small. For SKS and SKKS phases (Figure 1), we used events at distance ranges between 98°–126°, which ensures that SKS
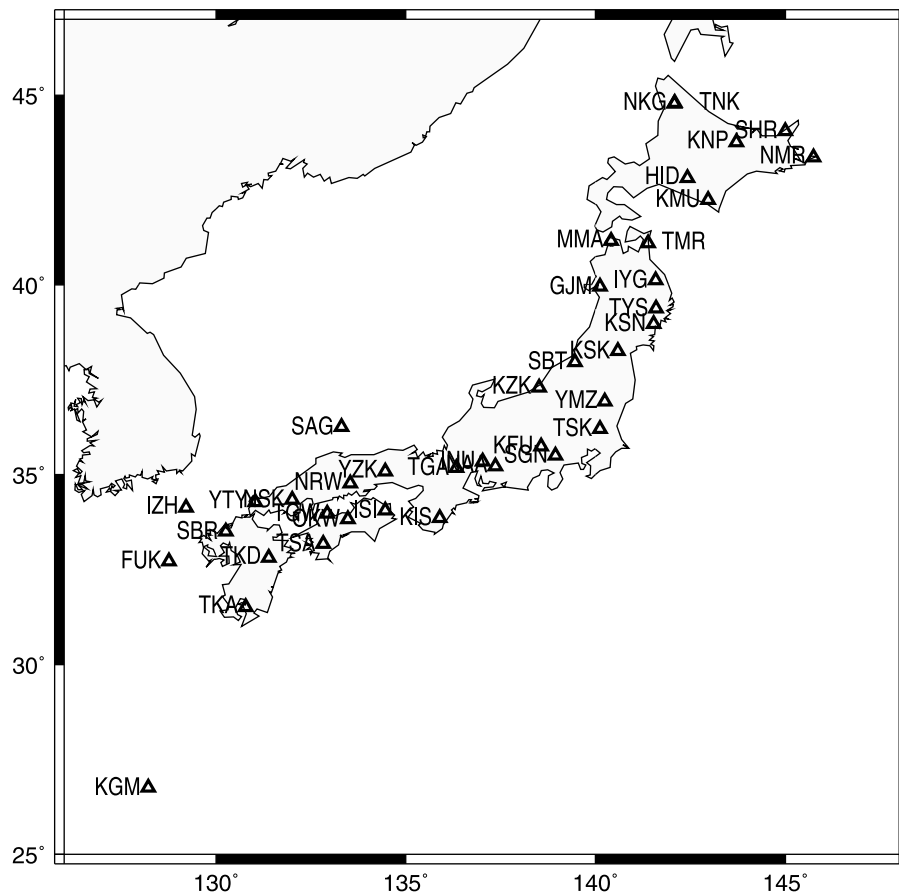

Figure 2. A map of F-net stations with station names labeled. Only stations used in this study are shown.

and SKKS have nearly the same raypath in the upper mantle on the receiver side and that both SKS and SKKS have significant amplitude. We used a magnitude threshold of Mw = 5.8 for all events. Initially, we examined ∼11,800 seismograms for SKS/SKKS and 226 seismograms for PcS/ScS. All records were visually inspected to ensure good waveform quality and high signal-to-noise ratios. Best fitting shear wave splitting parameters (ϕ, δt) were measured using multiple measurement methods simultaneously, since different methods can disagree for noisy data or complex or near-null splitting [e.g., *Wüstefeld and Bokelmann*, 2007; *Long and Silver*, 2009]. (All waveforms for which shear wave splitting measurements are presented in this paper are shown in the auxiliary material, including horizontal components in N-S/E-W and radial/transverse geometries.)[1]

[7] For the SKS/SKKS phases, we applied a 2-pass, 2-pole Butterworth bandpass filter with corner frequencies at 0.05 and 0.2 Hz to the data and visually selected arrivals with high signal-to-noise ratio for splitting analysis. Time windows for the splitting algorithm were chosen manually; they generally encompassed one full period of the wave and were optimized to identify the best-constrained splitting parameters. We identified records that had good arrivals for both SKS and SKKS for the same event-station pair and applied both the cross-correlation and the transverse component minimization splitting measurement methods [e.g., *Silver and Chan*, 1991] simultaneously using the SplitLab software [*Wüstefeld et al.*, 2008]. We only retained measurements in the data set for which the two measurement methods agreed within the 2σ formal errors and the errors were less than 30° for ϕ and 0.7 s for δt, and for which the transverse component signal-to-noise ratio was greater than ∼2. We also checked the shape of the transverse components for non-null SK(K)S arrivals; if the energy on the transverse component is due to anisotropy (and not mere noise), then the transverse component waveform should take the same shape as the time derivative of the radial component waveform [e.g., *Vinnik et al.*, 1989; *Chevrot*, 2000]. An example of such a comparison is shown in Figure S2 in the auxiliary material. For each splitting measurement, we computed 95% confidence regions derived from the formal errors estimated with the procedures described in the works by *Wüstefeld et al.* [2008] and *Silver and Chan* [1991].

[8] An example of a typical splitting measurement for an SKS arrival at station KNP (event Mw = 6.4, backazimuth = 55°, Δ = 104°) is shown in Figure 3. For this example, both the cross-correlation and transverse component minimization methods yield well-constrained estimates of the splitting parameters (ϕ = 15°, δt = 0.9 s). While the example shown in Figure 3 has a relatively high transverse component signal-to-noise ratio (SNR), it represents one of the noisier arrivals that we retained in the data set, and no arrivals with a transverse component SNR < 2 were retained. For relatively noisy arrivals, the fact that two different measurement methods yielded very similar splitting parameter estimates (Figure 3) gives additional confidence in the robustness of the results. We classified as null those arrivals that had high signal-to-noise ratio, good waveform clarity, and clearly linear initial uncorrected particle motion with a polarization aligned with the backazimuth.

[9] Our SKS/SKKS measurement procedure yielded a total of 53 SK(K)S phases for the same event-station pairs with well-constrained splitting parameters (either null or non-null) (Table 1). The station and event locations for these 53 pairs, along with the CMB pierce points on the receiver side, are shown in Figure 4. Unfortunately, the backazimuthal distribution is quite limited; all events are located in the Central America, Caribbean, or northern South America subduction zones, so the backazimuths in the SK(K)S data set only range from 35°–60°. The CMB pierce points for the SK(K)S phases sample the lowermost mantle just to the south and east of the Kamchatka peninsula (Figure 4), roughly beneath the Kurile and western Aleutian trenches.

[10] For the PcS/ScS phases, we applied a 2-pass, 2-pole Butterworth bandpass filter with corner frequencies at 0.1 and 1 Hz to the data and then followed the same preprocessing steps as for the SK(K)S phases. A slightly different filter was applied for the PcS/ScS arrivals than for SK(K)S, as the frequency content of the two types of phases was found to be slightly different. We applied both the cross-correlation and cross-convolution splitting measurement methods [*Menke and Levin*, 2003]; for the cross-convolution method, we assumed a single layer of anisotropy. For each measurement, we computed 95% confidence regions derived from the formal errors estimated with the procedures described in the work by *Menke and Levin* [2003] for the cross-convolution method and in the work by *Wüstefeld et al.* [2008] for the cross-correlation method. As with SK(K)S, we only retained well-constrained measurements for which the two
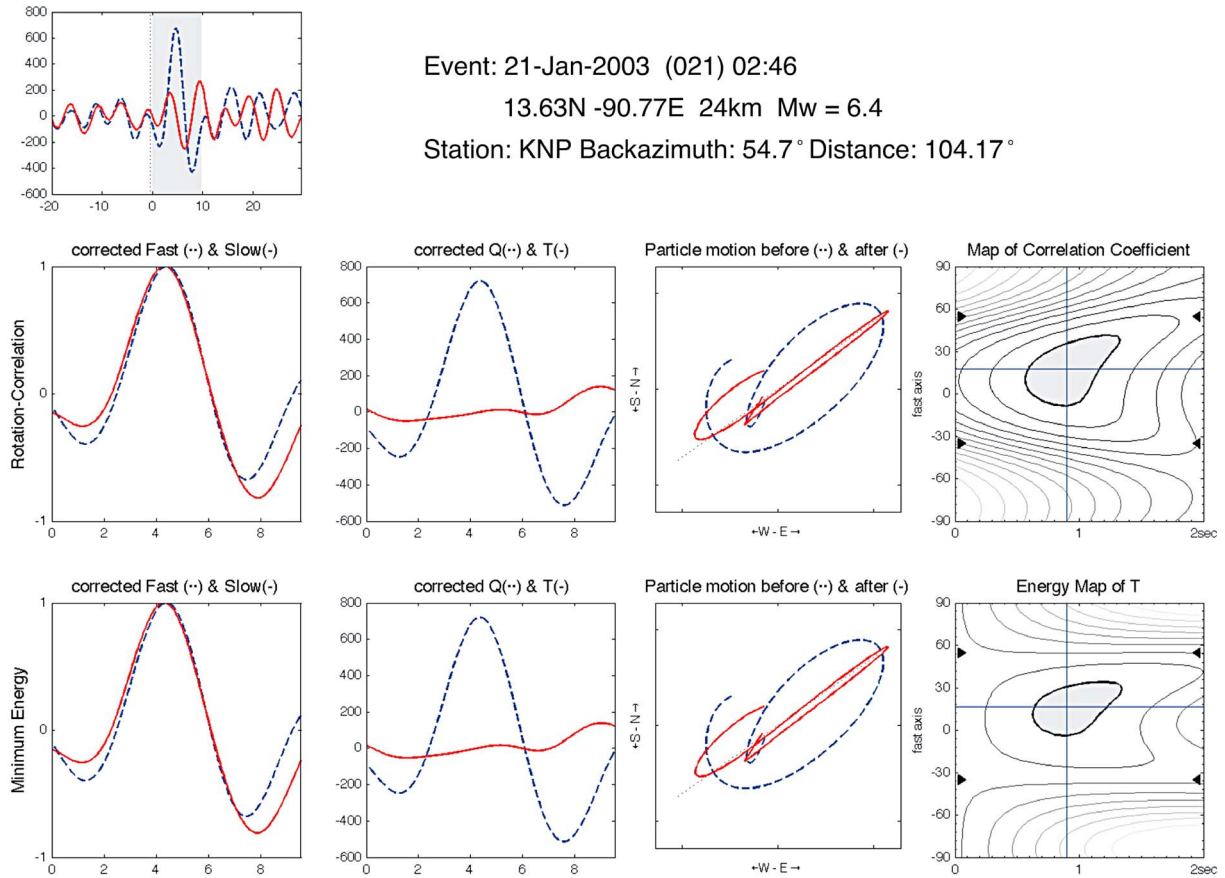
Figure 3. A typical example of SKS splitting measurements made using SplitLab for the transverse component minimization and cross-correlation methods at station KNP for an earthquake in the Central America subduction zone (Mw = 6.4, backazimuth = 54.7°, Δ = 104.17°). (top) The uncorrected radial (dashed blue line) and transverse (solid red line) components, along with the time window used in the splitting analysis (gray box). (middle row) The diagnostic plots for the cross-correlation method: from left, the fast (solid red) and slow (dashed blue) components, time-shifted to correct for the effect of splitting; the corrected radial (dashed blue) and transverse (solid red) components; the uncorrected (dashed blue) and corrected (solid red) particle motions; the correlation coefficients for all possible (ϕ, δt) pairs showing the 95% confidence region. (bottom row) Corresponding diagnostic plots for the transverse component minimization method. The splitting parameters obtained using both methods (ϕ = 15°, δt = 0.9 s) are consistent and generally well-constrained, despite the relatively high level of noise on the uncorrected transverse component waveform.

measurement methods agreed. Our initial strategy was to identify PcS and ScS phases for the same event-station pairs; however, we were not able to identify any pairs with well-constrained splitting parameters for both phases. This is likely due at least in part to the differences in P and S radiation patterns for any given earthquake source. Instead, we focused on measuring splitting for individual PcS and ScS phases at F-net stations where the splitting signal from upper mantle anisotropy beneath the receiver is relatively simple and well constrained (Category I and Category II stations from *Long and van der Hilst* [2005]). We obtained high-quality splitting measurements for 6 PcS and

7 ScS waveforms at 13 different F-net stations (Table 2). The distribution of earthquakes, stations, and CMB bounce points for PcS/ScS splitting measurements retained for interpretation are shown in Figure 5; these phases sample the D″ region more or less directly beneath Japan.

[11] An example of a typical splitting measurement for a PcS arrival at station NMR (backazimuth = 203°, Δ = 15°) is shown in Figure 6. For this example, both the cross-correlation and cross-convolution methods yield well-constrained estimates of the splitting parameters (ϕ = 39°, δt = 1.2 s). As we did for SKS/SKKS analyses, we classified as

Table 1. Splitting Results for SKS-SKKS Pairs in the F-net Data Set, Divided Into Category I, Category II, and Category III Pairs[a]

Station Name	Event (Year.Day)	BAZ (°)	SKS Splitting Parameters φ(°), δt(s)	SKKS Splitting Parameters φ(°), δt(s)	Upper Mantle Contribution φ(°), δt(s)	Corrected Splitting Parameters φ(°), δt(s)
			Category I			
FUK	**1999.166**	**47.96**	**Null**	**2 ± 15, 1.2 ± 0.3**	**−59, 1.13**	**−10 ± 15, 1.4 ± 0.6**
GJM	2007.253	48.63	Null	−3 ± 30, 1.1 ± 0.6		
HID	**2009.123**	**53.65**	**Null**	**−73 ± 6, 1.0 ± 0.2**	**−50, 0.28**	**−80 ± 10, 0.8 ± 0.2**
ISI	**1999.157**	**49.95**	**Null**	**−15 ± 12, 0.9 ± 0.4**	**50, 0.33**	**4 ± 15, 0.6 ± 0.5**
ISI	**2006.223**	**54.29**	**Null**	**−18 ± 11, 1.1 ± 0.5**	**50, 0.33**	**8 ± 16, 0.4 ± 0.4**
KNP	2003.021	54.77	15 ± 15, 0.9 ± 0.2	Null		
KNP	2007.164	54.68	−18 ± 5, 1.4 ± 0.4	Null		
KZK	**1999.273**	**55.30**	**Null**	**−17 ± 5, 1.6 ± 0.4**	**−38, 0.34**	**10 ± 15, 1.0 ± 0.2**
NAA	**2009.267**	**59.97**	**Null**	**−86 ± 6, 1.2 ± 0.2**	**−48, 0.39**	**−63 ± 20, 0.7 ± 0.4**
NKG	2007.164	53.16	−20 ± 4, 1.4 ± 0.3	Null		
SAG	2009.123	48.08	Null	2 ± 15, 0.6 ± 0.4		
SBR	**1999.157**	**46.63**	**Null**	**23 ± 6, 1.8 ± 0.3**	**−49, 0.38**	**10 ± 8, 1.8 ± 0.5**
SHR	2003.265	35.40	15 ± 5, 1.5 ± 0.4	Null		
SHR	2004.320	49.86	−10 ± 24, 0.8 ± 0.4	Null		
SHR	2007.164	55.65	Null	−15 ± 5, 1.7 ± 0.7		
SHR	2007.253	51.39	24 ± 6 1.4 ± 0.3	Null		
TGA	2009.123	50.91	18 ± 6, 1.3 ± 0.2	Null	−13, 0.54	
TNK	1997.245	45.53	5 ± 8, 1.1 ± 0.1	Null		
TSK	2007.164	53.81	Null	6 ± 14, 0.5 ± 0.4		
TYS	2004.325	53.74	−12 ± 7, 1.1 ± 0.4	Null		
YMZ	1999.157	53.59	Null	9 ± 15, 0.6 ± 0.2		
YMZ	2007.253	50.42	−6 ± 18, 0.9 ± 0.4	Null		
YTY	2006.223	51.82	−12 ± 6, 1.5 ± 0.5	Null		
YZK	2006.223	54.07	−1 ± 15, 0.5 ± 0.2	Null		
			Category II			
GJM	1999.157	52.6305	Null	Null		
ISI	**1997.142**	**54.5748**	**Null**	**Null**	**50, 0.33**	
IYG	2009.123	53.6143	Null	Null		
KGM	**2005.178**	**56.019**	**Null**	**Null**	**47, 0.58**	
KMU	2004.320	48.7063	Null	Null	−79, 0.59	
KNP	2004.320	48.7634	Null	Null		
KNP	2009.123	54.4859	Null	Null		
KSN	2007.253	50.5388	Null	Null		
MMA	**2004.320**	**46.7132**	**Null**	**Null**	**59, 0.38**	
NRW	2004.320	42.9699	Null	Null	−64, 1.09	
NSK	**2003.021**	**48.004**	**Null**	**Null**	**−30, 0.39**	
NSK	**2004.325**	**47.5685**	**Null**	**Null**	**−30, 0.39**	
NSK	**2006.223**	**52.5003**	**Null**	**Null**	**−30, 0.39**	
OKW	2009.267	57.6935	Null	Null		
SAG	2004.320	41.8638	Null	Null		
SBT	1999.166	54.582	Null	Null		
SBT	1999.273	55.8346	Null	Null		
SGN	**2004.320**	**48.1765**	**Null**	**Null**	**−48, 0.54**	
TGW	2009.267	57.3175	Null	Null		
TMR	2004.320	47.6959	Null	Null		
			Category III			
KNP	2003.237	54.7465	−12 ± 4, 1.0 ± 0.2	−65 ± 18, 0.5 ± 0.2		
KSK	**2004.320**	**48.3059**	**−18 ± 5, 0.7 ± 0.4**	**−5 ± 12, 0.9 ± 0.3**	**−34, 0.41**	**SKS: 6 ± 20, 0.4 ± 0.2; SKKS: 12 ± 18, 0.8 ± 0.4**

Table 1. (continued)

Station Name	Event (Year.Day)	BAZ (°)	SKS Splitting Parameters $\varphi(°)$, $\delta t(s)$	SKKS Splitting Parameters $\varphi(°)$, $\delta t(s)$	Upper Mantle Contribution $\varphi(°)$, $\delta t(s)$	Corrected Splitting Parameters $\varphi(°)$, $\delta t(s)$
SAG	2006.223	52.997	$30 \pm 12, 0.6 \pm 0.3$	$-13 \pm 5, 1.3 \pm 0.2$		
SHR	2003.021	55.7271	$5 \pm 30, 0.5 \pm 0.5$	$25 \pm 10, 0.9 \pm 0.2$		
TKA	**1997.142**	**52.6585**	**$12 \pm 10, 1.2 \pm 0.2$**	**$10 \pm 8, 1.6 \pm 0.3$**	**52, 0.63**	**SKS: $18 \pm 15, 1.1 \pm 13$; SKKS: $0 \pm 15, 1.8 \pm 0.5$**
TKD	1997.142	52.7362	$-12 \pm 5, 1.5 \pm 0.3$	$2 \pm 4, 1.6 \pm 0.2$		
TMR	1999.157	53.3475	$7 \pm 15, 0.5 \pm 0.1$	$2 \pm 18, 0.6 \pm 0.3$		
TYS	2004.320	48.7253	$-12 \pm 12, 1.2 \pm 0.4$	$-6 \pm 13, 1.2 \pm 0.5$		
TYS	2007.253	50.3877	$2 \pm 15, 0.7 \pm 0.6$	$12 \pm 15, 0.8 \pm 0.6$		

[a]Best fitting splitting parameters using the transverse component minimization method along with 2σ error bars for SK(K)S are shown, along with the expected splitting due to upper mantle anisotropy from *Long and van der Hilst* [2005] for those stations where it is well-constrained and simple. For Category I stations, those pairs for which the non-null SK(K)S splitting can be unambiguously attributed to anisotropy in the lowermost mantle are shown in bold. The last column shows splitting parameters for the split phase that have been explicitly corrected for the effect of upper mantle anisotropy beneath the receiver using the procedure described in the text. For Category II stations, pairs for which no upper mantle contribution is expected and a contribution from D″ anisotropy can be ruled out are shown in bold. For Category III stations, the pairs for which the SK(K)S splitting is inferred to be due to lowermost mantle anisotropy are shown in bold, along with splitting parameters that have been corrected for upper mantle anisotropy effects.

null those PcS arrivals that had high signal-to-noise ratio, good waveform clarity, and clearly linear initial uncorrected particle motion with a polarization aligned with the backazimuth. The same approach for splitting parameter estimation and null classification was also applied to ScS; an example of an ScS measurement is shown in Figure 7.

3. Results

[12] Our analysis yielded a total of 53 SKS-SKKS pairs, along with 6 PcS and 7 ScS measurements that can be compared with the known signature of upper mantle anisotropy at F-net stations. For ease of interpretation, we have divided the SKS-SKKS pairs into three categories (Table 1). In Category I

are those pairs which exhibit clearly and unambiguously discrepant splitting behavior, with one phase (SKS or SKKS) exhibiting null splitting and the other phase showing clear splitting with a well-constrained delay time of 0.5 s or greater. There are 24 SK(K)S pairs that fall into Category I; three examples of Category I pairs (waveforms and particle motions) are shown in Figure 8. In Category II are the pairs that exhibit null splitting for both SKS and SKKS; there are 20 pairs that fall into this category. In Category III are the pairs which yield well-constrained non-null splitting parameters for both SKS and SKKS. Of the 9 pairs that fall into this category, only two can be labeled as discrepant; for the remaining 7 pairs, the SKS and SKKS splitting parameters agree within the 2σ error bars.
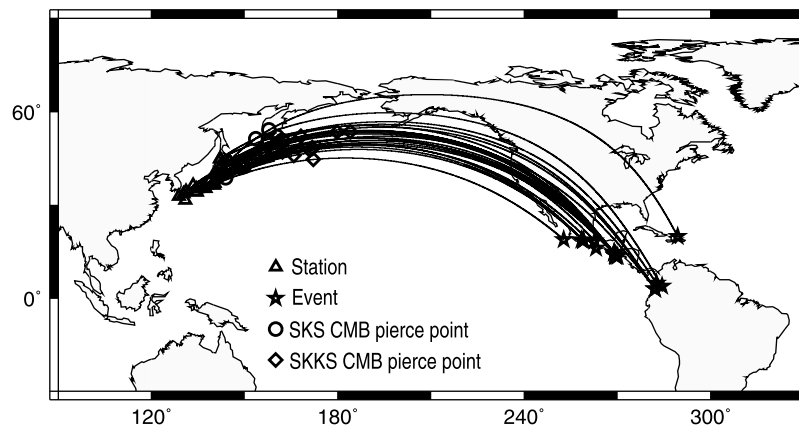

Figure 4. Event and station locations for the SK(K)S splitting analysis. Only those pairs for which we infer a contribution from D″ anisotropy are shown. F-net station locations are shown with triangles; event locations are shown with stars. Black lines denote great circle paths for the event-station pairs. Circles and diamonds show the core-mantle boundary pierce points for SKS and SKKS, respectively, for those pairs where we infer the presence of D″ anisotropy.

Table 2. Best Fitting Splitting Parameters and 2σ Error Bars Obtained Using the Cross-Correlation Method for PcS/ScS Arrivals in the Data Set, Along With the Expected Splitting Due to Upper Mantle Anisotropy Beneath the Station From *Long and van der Hilst* [2005][a]

Station Name	Event (Year.Day, Depth (km))	BAZ (°), Δ (°)	Splitting Parameters $\varphi(°)$, $\delta t(s)$	Used Phase	Upper Mantle Contribution	Corrected Splitting Parameters $\varphi(°)$, $\delta t(s)$
TSA	**2009.358, 410**	**8.81, 9.16**	**−18 ± 4, 1.35 ± 0.1**	**ScS**	**71, 0.27**	**−22 ± 4, 1.50 ± 0.2**
INU	2010.049, 577	327.64, 8.74	−46 ± 10, 1.35 ± 0.2	ScS		
TSK	1995.210, 444	193.15, 6.05	84 ± 2, 1.10 ± 0.1	ScS		
NAA	**1998.152, 411**	**218.89, 1.51**	**75 ± 10, 1.30 ± 0.2**	**ScS**	**−48, 0.39**	**99 ± 20, 0.90 ± 0.3**
IZH	2002.258, 586	2.74, 10.69	−4 ± 15, 1.10 ± 0.3	ScS		
TGW	2002.321, 525	29.06, 16.00	−48 ± 14, 1.20 ± 0.4	ScS		
KMU	2002.321, 525	9.98, 5.34	−42 ± 10, 1.15 ± 0.2	ScS	−79, 0.59	
KIS	2007.068, 436.2	349.59, 9.51	75 ± 10, 0.6 ± 0.2	PcS		
TKD	1999.339, 424	112.54, 6.76	−33 ± 2, 1.3 ± 0.1	PcS		
NMR	2002.214, 426.1	203.32, 15.07	39 ± 15, 1.2 ± 0.3	PcS	80, 0.72	
TNK	**1998.152, 411**	**204.85, 11.63**	**−61 ± 10, 1.7 ± 0.3**	**PcS**	**−13, 0.54**	**−39 ± 10, 1.2 ± 0.2**
KFU	1998.152, 411	229.29, 2.56	21 ± 10, 1.9 ± 0.4	PcS	−34, 0.79	
NAA	**2007.197, 315.6**	**308.04, 2.56**	**51 ± 10, 1.8 ± 0.4**	**PcS**	**−48, 0.39**	**73 ± 12, 1.95 ± 0.2**

[a]Measurements for which a significant contribution from upper mantle anisotropy can be ruled out are shown in bold. The last column shows splitting parameters for the split phase that have been explicitly corrected for the effect of upper mantle anisotropy beneath the receiver using the procedure described in the text.
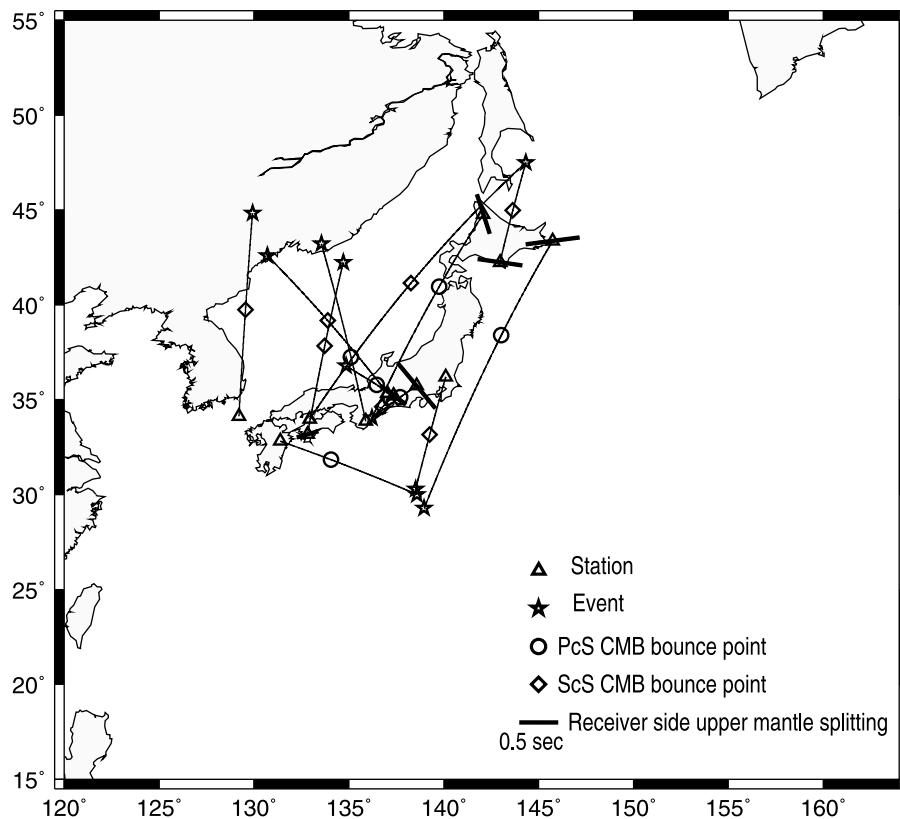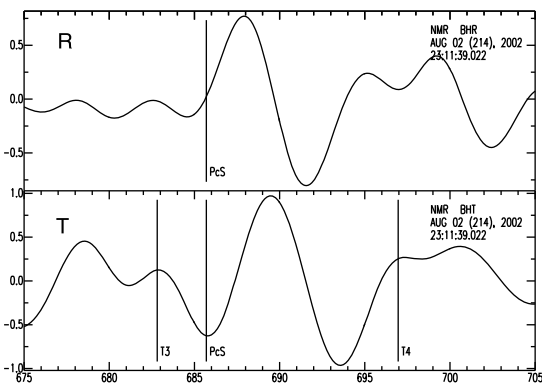

Figure 5. Event and station locations for the PcS/ScS splitting analysis. Event locations are shown with a star; stations are shown with a triangle. The CMB bounce points are shown with circles (PcS) or diamonds (ScS), along with great circle lines that link the station-event pairs. Short bars represent the orientation and magnitude of splitting due to upper mantle upper mantle anisotropy beneath the stations [*Long and van der Hilst*, 2005].
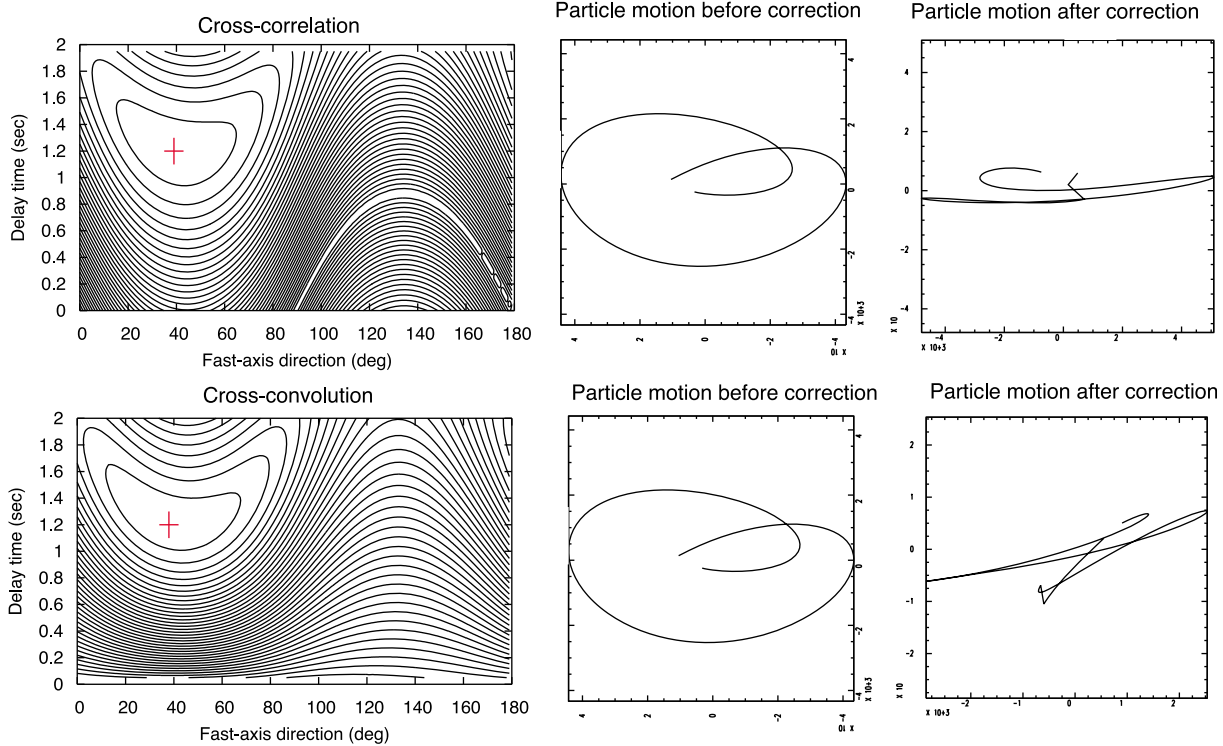
Figure 6. An example of a PcS splitting measurement using cross-correlation and cross-convolution methods at station NMR for an earthquake in the Japan subduction zone (backazimuth: 203.32°, epicentral distance: 15.07°). (top) The uncorrected radial and transverse components. (middle row) The diagnostic plots for the cross-correlation method: from left, map of cross-correlation coefficients, uncorrected particle motion, corrected particle motion. (bottom row) The corresponding diagnostic plots for the cross-convolution method. The splitting parameters obtained using both methods ($\phi = 39°$, $\delta t = 1.20$ s) are well constrained.

[13] Any consideration of possible contributions to PcS, ScS, and SK(K)S splitting from lowermost mantle anisotropy requires a detailed analysis of possible contributions to the observed splitting from anisotropy in the upper mantle beneath the receiver and (for ScS) from anisotropy close to the source. This analysis is undertaken in section 4. However, we first highlight a few first-order characteristics of the splitting data sets shown in Tables 1 and 2 that strongly suggest a significant contribution from anisotropy somewhere in the lower mantle, far away from the F-net stations. First, we note that our measured delay times for PcS and ScS phases (Table 2) are generally much larger than the known delay times due to upper mantle anisotropy beneath F-net stations [*Long and van der Hilst*, 2005]. This argues for a contribution to PcS/ScS splitting from somewhere else in the mantle; for PcS, this is likely in the lower mantle on the receiver side, but for ScS a contribution from the source side is possible as well. Second, the striking discrepancies in SKS and SKKS splitting for Category I pairs argues strongly
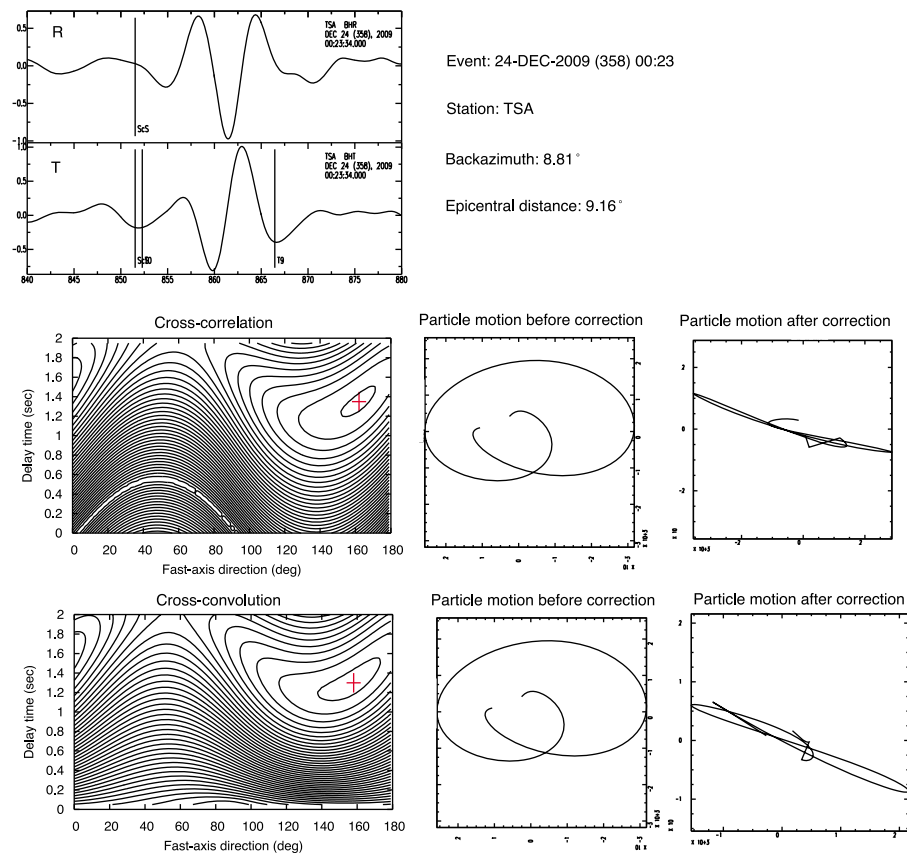
Figure 7. An example of ScS splitting measurements using cross-correlation and cross-convolution methods at station TSA for an earthquake in the Japan subduction zone (backazimuth: 8.81°, epicentral distance: 9.16°). (top) The uncorrected radial and transverse components. (middle row) The diagnostic plots for the cross-correlation method: from left, map of cross-correlation coefficients, uncorrected particle motion, corrected particle motion. (bottom row) The corresponding diagnostic plots for the cross-convolution method. The splitting parameters obtained using both methods ($\phi = 162°$, $\delta t = 1.35$ s) are well constrained.

for a contribution in the lowermost mantle on the receiver side, since SK(K)S phases have nearly identical paths in the upper mantle beneath the station (Figure 1) and only diverge significantly in the lowermost mantle [*Niu and Perez*, 2004; *Long*, 2009]. A third argument comes from the consistency in fast polarization directions measured for Category I pairs (Table 1); nearly all of the measured ϕ values trend roughly N-S. Because upper mantle anisotropy beneath Japan is very complex and varies spatially over short length scales [e.g., *Long and van der Hilst*, 2005], it is highly unlikely that these splitting observations are due to upper mantle anisotropy beneath the receivers. Rather, there is likely a coherent region of anisotropy somewhere in the deep mantle that is being sampled by the SK(K)S phases.

[14] One factor that may complicate the interpretation of the data set presented here is the possibility of frequency-dependent shear wave splitting.

Frequency-dependent splitting has been documented for several data sets [e.g., *Greve et al.*, 2008; *Wirth and Long*, 2010; *Long*, 2010] and is a consequence of lateral and/or depth heterogeneity in anisotropic structure [e.g., *Wirth and Long*, 2010]. In the presence of such heterogeneity, frequency-dependent splitting can complicate the interpretation, particularly when comparing splitting of different phases that may have difference frequency contents. This is particularly salient for Japanese data; several previous studies of ScS splitting in Japan exist [e.g., *Fukao*, 1984; *Tono et al.*, 2009] but differences in frequency content and filtering schemes among different studies make direct comparisons to our measurements difficult. The explicit investigation of frequency-dependent splitting is beyond the scope of this study, but we have taken several steps to ensure that the differences in splitting between different phases that we interpret in terms of lowermost mantle anisotropy are not due to frequency-dependent splitting. First, we have taken
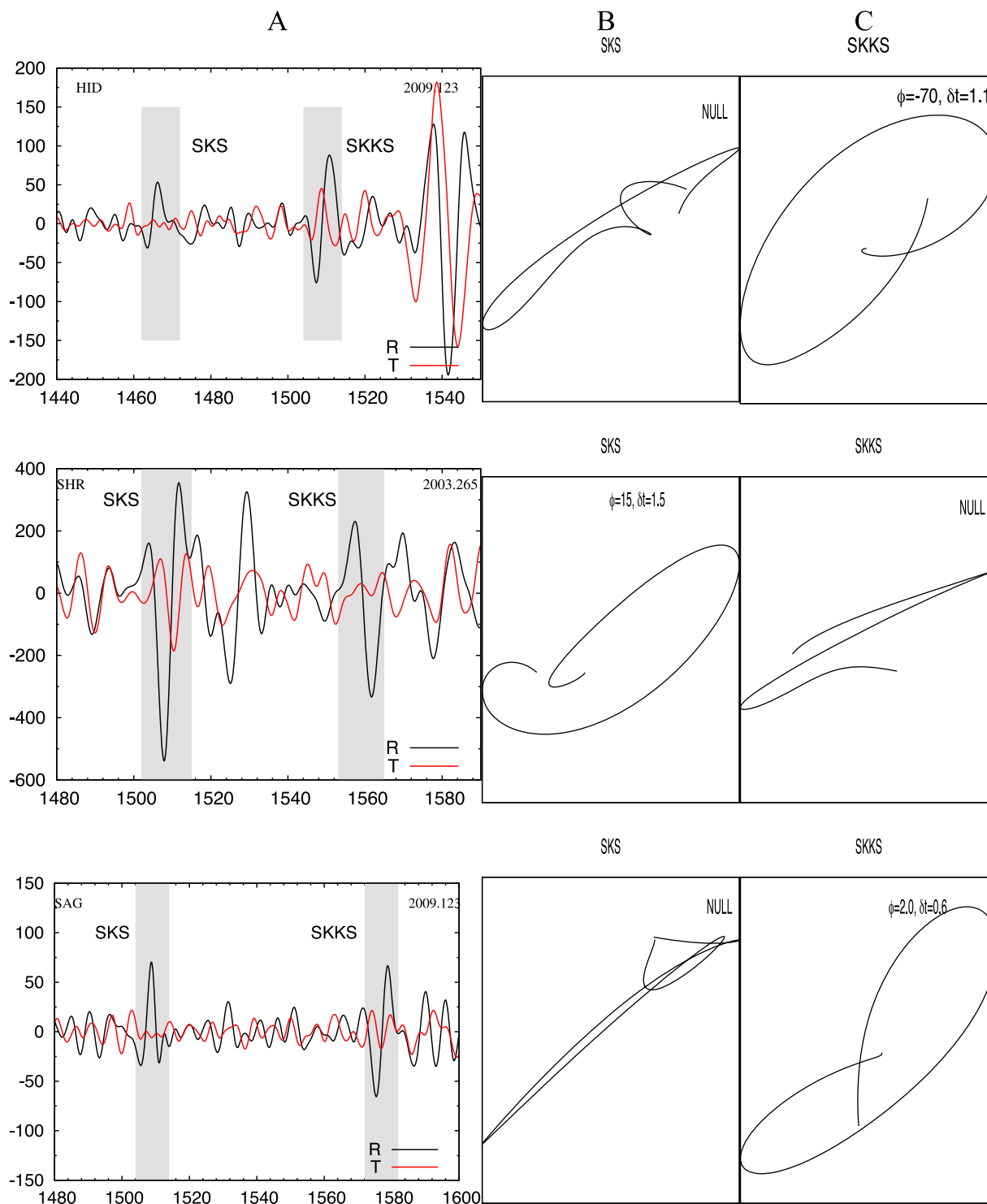
Figure 8. Radial and transverse SKS and SKKS seismograms and particle motion diagrams for a representative set of discrepant SKS-SKKS pairs from the full data set. (a) In this column, the radial (black line) and transverse (red line) components of SKS-SKKS waveform are shown, with the station name (upper left) and event data (year and Julian day, upper right). The shaded gray region indicated the time window used in the splitting analysis. (b and c) These columns show the corresponding particle motion diagram for SKS and SKKS, respectively. The best fitting splitting parameters (fast direction in degrees, delay time in sec) are shown in the upper right corner of the particle motion diagram; null and near-null measurements are indicated by "NULL."

care to check that the phases that are directly compared in this study (specifically SKS versus SKKS) have very similar frequency contents, with characteristic periods around ∼10 s. We have also taken care to ensure that the measurements of upper mantle anisotropy from *Long and van der Hilst* [2005] were carried out at similar frequencies as the SKS, SKKS, PcS, and ScS splitting measurements made for this study. Because we do not observe large, systematic differences in frequency content among the different phases that we are comparing in this study, we cannot attribute the observed differences in splitting to a frequency-dependent effect and instead infer a contribution from anisotropy in the lowermost mantle.

4. Interpretation: Discriminating and Locating Contributions From D″ Anisotropy

4.1. SKS/SKKS Phases

[15] In order to isolate the contribution to SK(K)S splitting from anisotropy in the D″ region, contributions to the observed splitting from elsewhere in the mantle must be carefully considered. First, we consider the simplest type of measurements to interpret: the 24 SKS/SKKS pairs in Category I, which exhibit null splitting for either the SKS or SKKS phase and non-null splitting for the other phase. Because the raypaths for SKS/SKKS are nearly identical in the upper mantle (Figure 1), it is very difficult to explain these large discrepancies in terms of upper mantle anisotropy, as it would require very large intrinsic anisotropy (as much as ∼50%) to cause a difference in splitting of ∼1.5 s with the very slight difference in propagation direction between SKS and SKKS in the upper mantle [*Long*, 2009]. Therefore, significant discrepancies in SKS and SKKS splitting for the same event/station pair require a contribution from anisotropy somewhere in the lower mantle on the receiver side [*Niu and Perez*, 2004; *Long*, 2009].

[16] As argued by *Long* [2009], the D″ region at the base of the mantle is the most likely location of the deep mantle anisotropy inferred from SKS-SKKS splitting discrepancies. The SKS and SKKS raypaths diverge most significantly at the base of the mantle (Figure 1), whereas in the transition zone and uppermost lower mantle, the first Fresnel zones of SK(K)S waves (corresponding to the region of greatest sensitivity [*Alsina and Snieder*, 1995; *Favier and Chevrot*, 2003]) with a ∼8–10 s characteristic period would overlap significantly. With

the exception of the D″ layer, the deeper parts of the lower mantle are thought to be generally isotropic, based on both mineral physics arguments [e.g., *Karato et al.*, 1995] and seismological observations [e.g., *Meade et al.*, 1995; *Panning and Romanowicz*, 2004]. Therefore, we argue that the most likely location of the anisotropic signal is in the D″ region at the base of the mantle, although we cannot completely rule out a contribution from elsewhere in the lower mantle.

[17] With these arguments in mind, we can map the regions of anisotropy in D″ beneath the northwestern Pacific that we infer from our SKS/SKKS measurements. Of the 24 discrepant SKS/SKKS pairs in Category I, seven were measured at stations where the upper mantle anisotropy signal is relatively simple (FUK, HID, ISI, KZK, NAA, and SBR), as argued by *Long and van der Hilst* [2005]. At these stations, we can evaluate (and rule out) any contribution to SK(K)S splitting from upper mantle anisotropy. At five of the six stations, the average upper mantle delay times observed using the splitting intensity measurement method are less than 0.5 s (Table 1). Such small delay times are likely below the detection threshold for the single-record measurement methods used in this study [see, e.g., *Long and Silver*, 2009] and are in any case smaller than most of the delay times that we observe for our non-null Category I arrivals, which range up to 1.5 s. For the remaining station (FUK), the upper mantle delay time is large (1.13 s), but the back-azimuth of our SK(K)S arrivals is roughly 90° from the upper mantle fast direction, and we do not expect any contribution to splitting from upper mantle anisotropy at this orientation. Therefore, for this subset of 10 SK(K)S pairs in Category I, highlighted in Table 1, the argument that the non-null splitting results from D″ anisotropy is very clear-cut.

[18] While the contribution to splitting from the relatively weak anisotropy in the upper mantle beneath the receiver is likely to be negligible for these pairs, we carried out an explicit correction for the effect of upper mantle anisotropy (where possible) and compared them to measurements made without upper mantle corrections. For the 10 Category I pairs which were measured at stations where the upper mantle anisotropy signal is well-understood and simple, we corrected the waveforms for the effect of upper mantle splitting and then re-measured the splitting parameters. Similar corrections have been carried out by many previous studies of D″ anisotropy [e.g., *Wookey et al.*, 2005; *Wookey and Kendall*, 2008; *Nowacki et al.*, 2010].
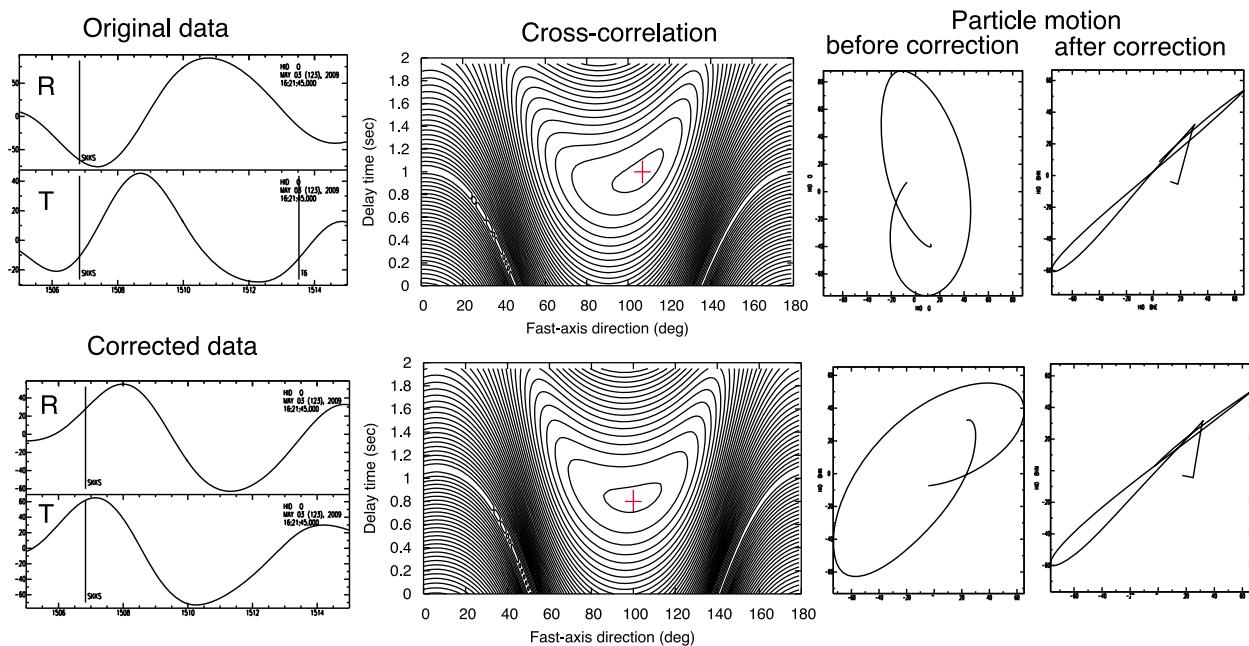
Figure 9. An example demonstrating the corrections for the upper mantle contribution to splitting. An SKKS phase from station HID (event 2009.123) has been analyzed. (top row) From left: original data of radial and transverse components, map of cross-correlation coefficients, particle motions before and after correction. (bottom) These figures correspond to the data which have been corrected for the contribution from upper mantle anisotropy (upper mantle splitting parameters for station HID: $\phi = -50°$, $\delta t = 0.28$ s). As this example demonstrates, for most arrivals in our data set the explicit correction for the effect of upper mantle anisotropy makes a negligible difference in our estimation of the D″-associated splitting parameters. For this example, we obtain lowermost mantle splitting parameters of $\phi = 107°$, $\delta t = 1.0$ s with no upper mantle correction; with the upper mantle correction, we obtain splitting parameters of $\phi = 100°$, $\delta t = 0.8$ s.

An example of the upper mantle correction is shown in Figure 9; for this pair (and indeed for all pairs), the measured splitting parameters are very similar for both the corrected and non-corrected waveforms. For all Category I pairs for which the upper mantle anisotropy signal is well known, the splitting parameters were measured after the upper mantle corrections and these measurements are shown in Table 1 and in map view in Figure 10.

[19] For the remaining 17 SK(K)S pairs in Category I, the possible contribution to splitting from upper mantle anisotropy beneath the receiver is more difficult to estimate; either the station in question was not included in the study by *Long and van der Hilst* [2005] or the station was found to have a very complicated upper mantle anisotropy signature which is not well represented by average splitting parameters. If we assume that the contribution from the upper mantle is negligible, as suggested by the generally small splitting intensities observed at F-net stations [*Long and van der Hilst*, 2005], then the simplest possible scenario for these 17 pairs is

that the non-null SK(K)S splitting we observe is due to D″ anisotropy, and these measurements are shown on the map in Figure 10 plotted at their CMB pierce points. As discussed above, the assumption that the non-null splitting of Category I pairs results from anisotropy in the D″ layer (and that any contribution from upper mantle anisotropy beneath the receivers is small) is supported by the generally consistent N-S fast directions observed for Category I pairs (Table 1 and Figure 10). This consistency is most compatible with a coherent region of anisotropy at the base of the mantle that is being sampled by SK(K)S phases at many different F-net stations, rather than anisotropy in the shallow part of the mantle beneath Japan, which is strongly variable [*Long and van der Hilst*, 2005].

[20] For the Category II arrivals, we do not observe any discrepancies in SKS/SKKS splitting and therefore we do not infer any contribution from D″ anisotropy for these arrivals. For a subset of 7 of the Category II arrivals where the contribution to SK(K)S splitting from the upper mantle is 1) known and 2)
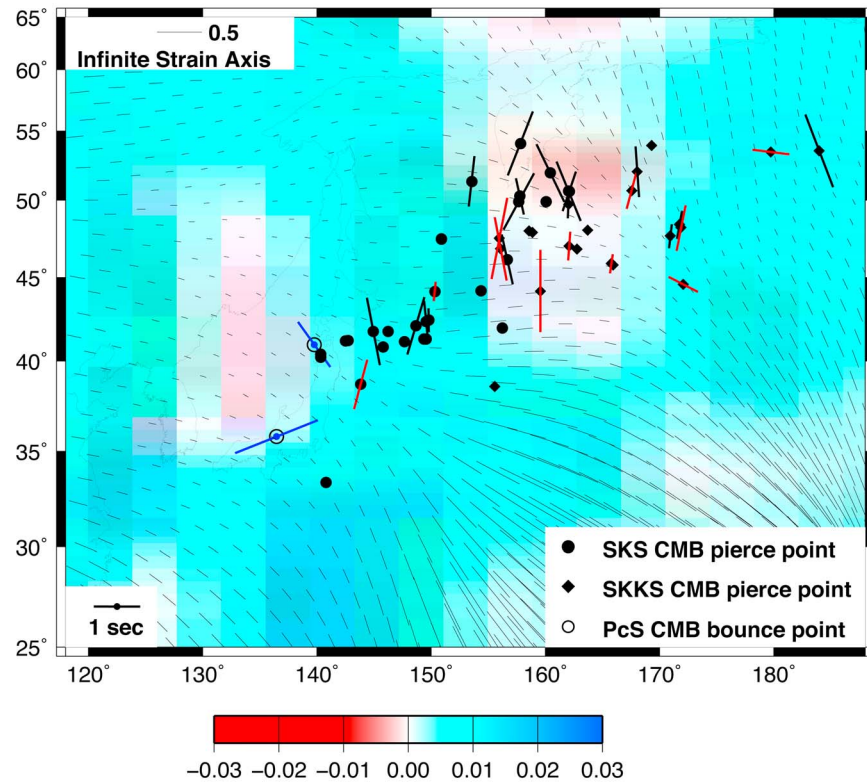
Figure 10. Summary map of the inferred contributions to SK(K)S and PcS splitting from D″ anisotropy. D″-associated splitting parameters are plotted as dark thick bars at the CMB pierce points (for SKS and SKKS phases) or bounce points (for PcS) the orientation and length of the bar correspond to (ϕ, δt) respectively. SK(K)S measurements that can be unequivocally attributed to D″ anisotropy are plotted in red; these measurements have been explicitly corrected for the effect of upper mantle anisotropy beneath the receiver. SK(K)S measurements which are likely (but not certainly) due to D″ anisotropy are plotted in black; these have not been corrected for the effect of the upper mantle. PcS measurements are plotted in blue and upper mantle anisotropy corrections have been applied. The black circles and diamonds shown without a fast axis direction represent SK(K)S pierce points for which a contribution from D″ anisotropy can be ruled out. Background colors correspond to isotropic S wave speeds at the base of the mantle from the model of *Houser et al.* [2008], plotted as relative deviations from a reference model. The thin light bars indicate the direction and magnitude of the infinite strain axis (ISA) from the model of *Conrad and Behn* [2010]. A map showing lines linking the SKS and SKKS CMB pierce points for all SKS-SKKS pairs in the data set may be found in Figure S1 in the auxiliary material.

expected to be small (either because the upper mantle delay times are less than ~0.5 s or because the backazimuth is aligned with a nodal plane), we can actually use the observation of null splitting for both SKS and SKKS to rule out a contribution from D″ anisotropy for these arrivals. These 7 pairs, observed at 5 different F-net stations (ISI, KGM, MMA, NSK, and SGN), are highlighted in Table 1 and are plotted on the map in Figure 10 at their CMB pierce points; for these regions, we can explicitly rule out any contribution from D″ anisotropy to SK(K)S phases. For the rest of the Category II arrivals, it is difficult to completely rule out a contribution from the lowermost mantle, because the possible effect of upper mantle anisotropy on the SK(K)S waveforms is not well known.

[21] The Category III pairs are slightly more difficult to interpret than the Category I and II pairs, because both the SKS and SKKS arrivals exhibit significant splitting (Table 1) and for most of the pairs in this category (seven out of nine) the upper mantle anisotropy contribution is not well constrained (the exceptions are at stations KSK and TKA). Of the nine Category III pairs in the data set, only two exhibit SKS/SKKS splitting discrepancies (at stations KNP and SAG; see Table 1), with fast directions that are (statistically significantly) different but similar delay times. This difference is likely due to some effect of D″ anisotropy on either the SKS or the SKKS phase (or both), but because the upper mantle anisotropy signal is not well known the location, strength, and geometry of D″
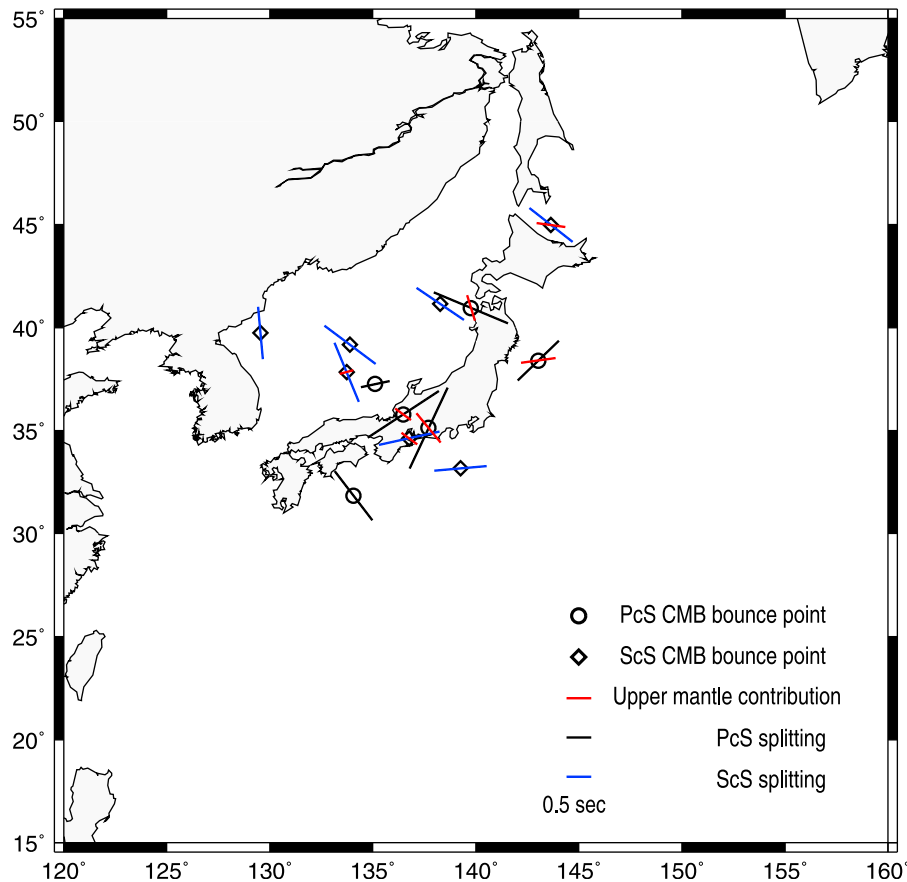
Figure 11. Map of PcS and ScS splitting observed in this study compared to the expected splitting due to upper mantle anisotropy beneath each station from *Long and van der Hilst* [2005]. All measurements are plotted at the CMB bounce points of PcS (circles) and ScS (diamonds). ScS splitting measurements are shown as blue. Black bars indicate PcS splitting measurements, and red bars denote the corresponding upper mantle splitting signal for each station.

cannot be constrained for these arrivals. However, we can confidently infer a contribution from D″ anisotropy to both SKS and SKKS splitting for the two Category III pairs for which the splitting due to upper mantle anisotropy can be predicted (at stations KSK and TSA). At station KSK (see Table 1), the upper mantle fast direction ($\phi = -34°$) is 83° from the SK(K)S backazimuth (baz = 48°); this close to the 90° nodal plane, we do not expect a large contribution to SK(K)S splitting from upper mantle anisotropy. A similar argument can be made for the SK(K)S pair observed at station TKA, where the upper mantle fast direction ($\phi = 52°$) is identical to the backazimuth. Even though we expect any contribution from upper mantle anisotropy to be small, we did carry out an explicit correction for the upper mantle signal for these two pairs and the corrected splitting is measured and shown in Table 1. For these two Category III pairs, therefore, we infer that the splitting for both SKS and SKKS is due to anisotropy at the base of the mantle, and these

measurements (corrected for the effect of upper mantle anisotropy) are plotted in red at their CMB pierce points on the map in Figure 10.

4.2. PcS/ScS Phases

[22] The interpretation of our measurements of PcS and ScS splitting is, unfortunately, less clear-cut than for SKS/SKKS splitting, because we did not identify any PcS/ScS phases from the same event-station pairs. However, we can still examine each of the 6 PcS and 7 ScS arrivals in our data set and compare their measured splitting parameters to the splitting expected from upper mantle anisotropy. This comparison is shown in Table 2 and plotted in map form in Figure 11. For simplicity, we have plotted both the ScS/PcS splitting and (for comparison) the expected upper mantle splitting signal at the CMB bounce point for the phase; however, this plotting convention assumes that there is a contribution from D″ anisotropy, which may not be the case for all arrivals.
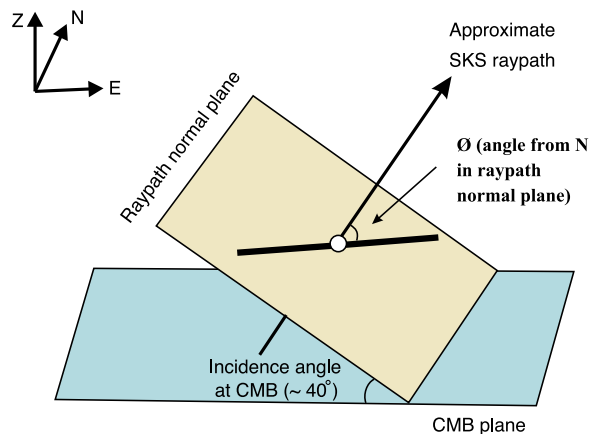
Figure 12. A sketch of the raypath geometry above the CMB and the geometry of the fast splitting direction in the D″ layer inferred from the anomalous SKKS splitting measurements presented in this study, modified from *Long* [2009].

[23] It is evident from the comparison between ScS/PcS splitting and the known upper mantle splitting signal that for many of the ScS/PcS arrivals, there is a contribution to splitting that cannot be explained by upper mantle anisotropy and must result from anisotropy elsewhere in the mantle. We identified seven out of the 13 ScS/PcS arrivals that exhibit significant discrepancies between the measured splitting and the expected upper mantle splitting; in which, these four arrivals are highlighted in Table 2. These four arrivals were selected because either the upper mantle splitting beneath the station has a small delay time (<0.5 s) or, in the case of the arrivals at station TNK, the observed PcS delay time is more than three times larger than the expected upper mantle signal (1.7–1.8 s for PcS versus 0.54 s for the upper mantle). For the other six PcS/ScS arrivals in the data set, we do not know the upper mantle anisotropy. It is very interesting to note that the seven measured ScS splitting delay times are very consistent, varying from 1.1 s to 1.35 s, while splitting varies from 0.6 s to 1.9 s for PcS.

[24] Of the four arrivals that exhibit significant discrepancies with the expected splitting due to upper mantle anisotropy beneath the station, two are PcS phases and the remaining two are ScS phases. For the two discrepant PcS arrivals, we argue (as we did for SK(K)S phases above) that the most likely source of the anisotropy is in the D″ layer at the base of the mantle, and we plot these two splitting measurements (explicitly corrected for any upper mantle contribution, as for SK(K)S; see Table 2) at their CMB bounce points on the map in Figure 10 which summarizes the inferred locations of D″ anisotropy.

For the two ScS arrivals, there is more ambiguity in the interpretation, because a possible contribution to splitting from anisotropy in the vicinity of the earthquake source must be considered. We restricted our PcS/ScS splitting analysis to events deeper than 300km, as the contribution to shear wave splitting from anisotropy deeper than that has been generally thought to be minimal and is often ignored in studies of D″ anisotropy [see, e.g., *Fouch et al.*, 2001; *Thomas and Kendall*, 2002; *Garnero et al.*, 2004; *Rokosky et al.*, 2004; *Usui et al.*, 2005; *Ford et al.*, 2006]. However, several recent studies have suggested a contribution to shear wave splitting from anisotropy near the source (in the deep upper mantle, the transition zone, or the uppermost lower mantle) for events deeper than 300 km [*Chen and Brudzinski*, 2003; *Wookey and Kendall*, 2004; *Wookey et al.*, 2005; *Foley and Long*, 2011]. For example, *Foley and Long* [2011] identified significant source-side splitting (~1 s or more) for deep events (>300 km) in the Tonga subduction zone. Because of the possibility of a contribution from anisotropy near the source, we cannot say with confidence that the six ScS phases that exhibit anomalous splitting reflect anisotropy in the D″ region, although we can be confident that there is a contribution either from D″ or from near-source anisotropy (or both). Future studies of source-side shear wave splitting for the Japan and Izu-Bonin subduction zones (the source regions for these earthquakes) using phases that do not sample the D″ region, such as direct teleseismic S, should be able to distinguish between these possibilities.

5. Discussion

[25] Splitting parameters measured for PcS, ScS, SKS, and SKKS arrivals at F-net stations, in combination with previously published estimates of upper mantle anisotropy beneath Japan, provide unequivocal evidence for anisotropic structure in the lowermost mantle beneath the northwestern Pacific, most likely in the D″ layer. The splitting parameters (ϕ, δt) associated with D″ anisotropy, shown in map view in Figure 10, can shed some light on the geometry and strength of anisotropy (and perhaps deformation) at the base of the mantle. For SK(K)S phases that sample D″ to the south and east of Kamchatka, the typical delay times of ~1.0–1.5 s corresponds to ~1–2% anisotropy if the anisotropy is distributed throughout the D″ layer and a path length of ~350–400 km is assumed. This estimate of anisotropy strength is consistent with

what has been inferred from other studies [e.g., *Wookey and Kendall*, 2007, and references therein]. The striking preponderance of generally N-S fast directions observed in the SK(K)S data set (Figure 10) suggests that the geometry of the anisotropy is fairly uniform throughout the region sampled by our data. We can explicitly compare our measurements with a complementary data set obtained by *Wookey et al.* [2005], who sampled a region of D″ beneath the Pacific Ocean that partially overlaps with our study region. First, it is important to consider the raypath geometry of the SK(K)S phases shown in our data set. As shown in Figure 12, the incidence angle for SK(K)S phases is ~40°, which means that the roughly N-S fast directions measured in our study must actually be considered in a 3-D geometry. Our inferred geometry is roughly consistent with the observations of *Wookey et al.* [2005], who observed fast shear wave axes that dip strongly to the NW (J. Wookey, personal communication, 2011) using differential S-ScS splitting.

[26] The PcS phases that we infer to have sampled D″ anisotropy beneath Japan (Figures 10 and 11) do not exhibit the N-S fast directions that are observed for the SK(K)S data set, which may indicate that the deformation geometry in D″ beneath Japan is different than that beneath the Kurile-Aleutian region. The strength of D″ anisotropy beneath Japan may also be different; the average PcS delay time of 1.5 s is somewhat larger than the average of 1.2 s for the most robust SK(K)S measurements. (Given the small number of PcS measurements that we can confidently interpret in terms of D″ anisotropy, however, these suggestions are far from certain.)

[27] What is a plausible model to explain our observations of lowermost mantle anisotropy beneath the northwestern Pacific? Because our SK(K)S data set is larger and easier to interpret, we focus on these observations, which sample D″ to the south and east of Kamchatka (Figure 10). Two different types of models have been proposed to explain D″ anisotropy; one invokes the shape preferred orientation (SPO) of elastically distinct materials and the other invokes the crystallographic or lattice preferred orientation (LPO) of intrinsically anisotropic minerals. We examine the plausibility of each hypothesis in the context of our observations beneath Kamchatka.

[28] In the SPO model, D″ anisotropy could be produced by the alignment of inclusions of material with elastic properties distinct from the surrounding matrix, such as pockets of partial melt or materials

from subducting slabs that have reached the CMB [*Kendall and Silver*, 1998]. However, this type of model seems somewhat unlikely for our study region. An isotropic whole mantle shear wave velocity model [*Houser et al.*, 2008] does not show particularly low velocities throughout our study region, as might be expected if the D″ layer had significant partial melt throughout. Nor do we necessarily expect subducted slab remnants to be present in the lowermost mantle here; a recent study by *van der Meer et al.* [2010] that interrogated tomographic models of the mantle for the signatures of subducting slabs at depth argues against the presence of slab remnants beneath Kamchatka. Finally, forward modeling work by *Hall et al.* [2004] suggests that SPO-type models for D″ anisotropy are inefficient at generating splitting of SK(K)S phases.

[29] Alternatively, solid-state deformation in D″ beneath Kamchatka could result in the lattice preferred orientation of lowermost mantle minerals; the most likely candidate minerals to contribute to D″ anisotropy are post-perovskite [e.g., *Oganov et al.*, 2005; *Yamazaki et al.*, 2006; *Merkel et al.*, 2007; *Miyagi et al.*, 2010; *Mao et al.*, 2010], ferropericlase (magnesiowüstite) [e.g., *Yamazaki and Karato*, 2002; *Long et al.*, 2006; *Marquardt et al.*, 2009], or a combination of both. It has been argued that (Mg,Fe)O may make the stronger contribution to LPO-induced D″ anisotropy even though volumetrically it is less important than (post-)perovskite; it is likely the weaker phase and may accommodate more strain [e.g., *Karato*, 1989; *Madi et al.*, 2005] and its intrinsic anisotropy at D″ pressures is very high, particularly for increased iron contents [*Marquardt et al.*, 2009]. Some authors have argued that observations of anisotropy in the D″ layer are more consistent with LPO of post-perovskite [e.g., *Nowacki et al.*, 2010], while others have argued that either post-perovskite or ferropericlase LPO can explain seismological observations [e.g., *Wenk et al.*, 2011]. In any case, our ability to correctly predict the effective anisotropy for assemblages of lowermost mantle minerals is hampered by our incomplete knowledge of dominant slip systems at D″ conditions and uncertainties in the single-crystal elastic constants for ferropericlase and (especially) post-perovskite at very high pressures.

[30] These limitations make quantitative predictions of shear wave splitting for different deformation scenarios in our study region difficult. However, it is still instructive to compare the geometry of our observed SK(K)S splitting to the deformation predicted by a mantle convection model. As shown in Figure 10, we compare our observed N-S fast axes

beneath Kamchatka to the infinite strain axis (ISA) predictions in the lowermost mantle from the model of *Conrad and Behn* [2010]; this is an instantaneous global mantle flow calculation that models flow due to density heterogeneities predicted from a seismic tomography model. Strikingly, our observations do not agree well with the predictions of *Conrad and Behn*'s [2010] model, at least if we assume that a simple relationship between strain and anisotropy holds throughout the study region. In the eastern part of our region of inferred D″ anisotropy, the ISA directions are roughly N-S, similar to our measured fast directions, but to the west, there is a transition in the ISA directions to E-W while the fast splitting directions remain dominantly N-S. Of course, since the relationship between strain and anisotropy for a realistic lowermost mantle aggregate is not well known, we cannot predict with certainty what relationship we would expect between ϕ and the ISA direction. The difficulty in comparing the ISA directions to our fast axis observations is compounded by the complex geometry of SK(K)S raypaths above the CMB (Figure 12); because the incidence angle of the rays is ~40°, it is not straightforward to compare the map projection of the SK(K)S fast axis shown in Figure 10 with the ISA directions in the horizontal plane computed by *Conrad and Behn* [2010]. Despite these limitations, however, the fact that there is a striking transition in deformation geometry predicted by *Conrad and Behn*'s [2010] model for our study region that is not seen in our splitting observations is notable.

[31] Because instantaneous mantle flow calculations are very sensitive to the tomographic model used as input and the resolution of global tomography models is generally poor in the lower mantle [e.g., *Bull et al.*, 2010], it may be that the flow geometry at the base of the mantle beneath our study region is different than that predicted by the preferred model of *Conrad and Behn* [2010]. Indeed, a recent study by *Walker et al.* [2011] examined a range of global mantle flow models and compared them to observations of D″ anisotropy; a visual comparison among the different flow models used in this study indicates some differences, and depending on the assumptions made about the mechanisms for LPO anisotropy, differences in the predicted anisotropy structure are present as well. Additionally, as discussed above, the comparison between the measured fast directions we attribute to D″ anisotropy and the ISA directions computed by *Conrad and Behn* [2010] is not entirely straightforward. Taken at face value, however, the comparison shown in Figure 10 suggests that there may be a transition in the mechanism and/or geometry of LPO within our study region, perhaps due to lateral variations in thermochemical structure.

6. Summary

[32] We have measured shear wave splitting parameters for PcS, ScS, SKS, and SKKS phases using broadband data from the Japanese F-net array. In combination with previously published estimates of upper mantle anisotropy beneath these stations, these measurements enable us to investigate seismic anisotropy at the base of the mantle beneath the northwestern Pacific Ocean. For SK(K)S phases measured for the same event-station pairs that sample the D″ layer to the south and east of the Kamchatka peninsula, we observed pronounced discrepancies between SKS and SKKS splitting, as well as examples of SK(K)S splitting that are not consistent with the known upper mantle anisotropy beneath the stations. This anomalous splitting, which we attribute to anisotropy in the D″ region, exhibits delay times between ~0.5–1.5 s and fast directions that generally trend N-S. We infer a fairly large region of coherent anisotropy (and thus deformation) in the D″ layer that is sampled by SK(K)S phases in our data set. Constraints on D″ anisotropy from PcS/ScS phases are weaker than those provided by SK(K)S, but we have identified three PcS arrivals which likely reflect D″ anisotropy beneath Japan, and an additional six ScS arrivals which reflect anisotropy in the D″ layer, in the mantle close to the earthquake source, or a combination of these. Our preferred model to explain our observations is that there is a large region of coherent mantle flow and deformation beneath the northwestern Pacific which induces the lattice preferred orientation of lowermost mantle minerals, resulting in seismic anisotropy that is sampled by SK(K)S arrivals in the F-net data set.

Acknowledgments

References

Alsina, D., and R. Snieder (1995), Small-scale sublithospheric continental mantle deformation: Constraints from SKS splitting observations, *Geophys. J. Int.*, *123*, 431–448, doi:10.1111/j.1365-246X.1995.tb06864.x.

Bull, A. L., A. K. McNamara, T. W. Becker, and J. Ritsema (2010), Global scale models of the mantle flow field predicted by synthetic tomography models, *Phys. Earth Planet. Inter.*, *182*, 129–138, doi:10.1016/j.pepi.2010.03.004.

Chen, W.-P., and M. R. Brudzinski (2003), Seismic anisotropy in the mantle transition zone beneath Fiji-Tonga, *Geophys. Res. Lett.*, *30*(13), 1682, doi:10.1029/2002GL016330.

Chevrot, S. (2000), Multichannel analysis of shear wave splitting, *J. Geophys. Res.*, *105*, 21,579–21,590, doi:10.1029/2000JB900199.

Conrad, C. P., and M. D. Behn (2010), Constraints on lithosphere net rotation and asthenospheric viscosity from global mantle flow models and seismic anisotropy, *Geochem. Geophys. Geosyst.*, *11*, Q05W05, doi:10.1029/2009GC002970.

Favier, N., and S. Chevrot (2003), Sensitivity kernels for shear wave splitting in transverse isotropic media, *Geophys. J. Int.*, *153*, 213–228, doi:10.1046/j.1365-246X.2003.01894.x.

Foley, B. J., and M. D. Long (2011), Upper and mid-mantle anisotropy beneath the Tonga slab, *Geophys. Res. Lett.*, *38*, L02303, doi:10.1029/2010GL046021.

Ford, S. R., E. J. Garnero, and A. K. McNamara (2006), A strong lateral shear velocity gradient and anisotropy heterogeneity in the lowermost mantle beneath the southern Pacific, *J. Geophys. Res.*, *111*, B03306, doi:10.1029/2004JB003574.

Fouch, M. J., M. K. Fischer, and M. E. Wysession (2001), Lowermost mantle anisotropy beneath the Pacific: Imaging the source of the Hawaiian plume, *Earth Planet. Sci. Lett.*, *190*, 167–180, doi:10.1016/S0012-821X(01)00380-6.

Fukao, Y. (1984), Evidence from core-reflected shear waves for anisotropy in the Earth's mantle, *Nature*, *309*, 695–698, doi:10.1038/309695a0.

Garnero, E. J., and A. K. McNamara (2008), Structure and dynamics of Earth's lower mantle, *Science*, *320*, 626–628, doi:10.1126/science.1148028.

Garnero, E. J., and M. S. Thorne (2007), Earth's ULVZ: Ultra-low velocity zone, in *Encyclopedia of Geomagnetism and Paleomagnetism*, edited by D. Gubbins and E. Herrero-Bervera, pp. 970–973, Springer, Dordrecht, Netherlands, doi:10.1007/978-1-4020-4423-6_309.

Garnero, E. J., V. Maupin, T. Lay, and M. J. Fouch (2004), Variable azimuthal anisotropy in Earth's lowermost mantle, *Science*, *306*, 259–261, doi:10.1126/science.1103411.

Greve, S. M., M. K. Savage, and S. D. Hofmann (2008), Strong variations in seismic anisotropy across the Hikurangi subduction zone North Island, New Zealand, *Tectonophysics*, *462*, 7–21, doi:10.1016/j.tecto.2007.07.011.

Hall, S. A., J.-M. Kendall, and M. van der Baan (2004), Some comments on the effects of lower-mantle anisotropy on SKS and SKKS phases, *Phys. Earth Planet. Inter.*, *146*, 469–481, doi:10.1016/j.pepi.2004.05.002.

Hernlund, J. W., C. Thomas, and P. J. Tackley (2005), A doubling of the post-perovskite phase boundary and structure of the Earth's lowermost mantle, *Nature*, *434*, 882–886, doi:10.1038/nature03472.

Houser, C., G. Masters, P. Shearer, and G. Laske (2008), Shear and compressional velocity models of the mantle from cluster analysis of long-period waveforms, *Geophys. J. Int.*, *174*, 195–212, doi:10.1111/j.1365-246X.2008.03763.x.

Karato, S. (1989), Plasticity-crystal structure systematics in dense oxides and its implications for the creep strength of the Earth's deep interior: A preliminary result, *Phys. Earth Planet. Inter.*, *55*, 234–240, doi:10.1016/0031-9201(89)90071-X.

Karato, S. (1998), Some remarks on the origin of seismic anisotropy in the D″ layer, *Earth Planets Space*, *50*, 1019–1028.

Karato, S., S. Zhang, and H.-R. Wenk (1995), Superplasticity in the Earth's lower mantle: Evidence from seismic anisotropy and rock physics, *Science*, *270*, 458–461, doi:10.1126/science.270.5235.458.

Karki, B. B., R. M. Wentzcovitch, S. de Gironcoli, and S. Baroni (1999), First principles determination elastic anisotropy and wave velocities of MgO at lower mantle conditions, *Science*, *286*, 1705–1707, doi:10.1126/science.286.5445.1705.

Kendall, J. M., and P. G. Silver (1996), Constraints from seismic anisotropy on the nature of the lower mantle, *Nature*, *381*, 409–412, doi:10.1038/381409a0.

Kendall, J.-M., and P. G. Silver (1998), Investigating causes of D″ anisotropy, in *The Core-Mantle Boundary Region*, *Geodyn. Ser.*, vol. 28, edited by M. Gurnis et al., pp. 97–118, AGU, Washington D. C.

Lay, T., and E. J. Garnero (2007), Reconciling the post-perovskite phase with seismological observations of lowermost mantle structure, in *Post-Perovskite, The Last Mantle Phase Transition*, *Geophys. Monogr. Ser.*, vol. 174, edited by K. Hirose et al., pp. 129–153, AGU, Washington, D. C.

Lay, T., Q. Williams, E. J. Garnero, L. Kellogg, and M. E. Wysession (1998), Seismic wave anisotropy in the D″ region and its implications, in *The Core-Mantle Boundary Region*, *Geodyn. Ser.*, vol. 28, edited by M. Gurnis et al., pp. 299–318, AGU, Washington, D. C.

Lay, T., E. J. Garnero, and S. A. Russell (2004), Lateral variation of the D″ discontinuity beneath the Cocos Plate, *Geophys. Res. Lett.*, *31*, L15612, doi:10.1029/2004GL020300.

Long, M. D. (2009), Complex anisotropy in D″ beneath the eastern Pacific from SKS–SKKS splitting discrepancies, *Earth Planet. Sci. Lett.*, *283*, 181–189, doi:10.1016/j.epsl.2009.04.019.

Long, M. D. (2010), Frequency-dependent shear wave splitting and heterogeneous anisotropic structure beneath the Gulf of California region, *Phys. Earth Planet. Inter.*, *182*, 59–72, doi:10.1016/j.pepi.2010.06.005.

Long, M. D., and P. G. Silver (2009), Shear wave splitting and mantle anisotropy: Measurements, interpretations, and new directions, *Surv. Geophys.*, *30*, 407–461, doi:10.1007/s10712-009-9075-1.

Long, M. D., and R. D. van der Hilst (2005), Upper mantle anisotropy beneath Japan from shear wave splitting, *Phys. Earth Planet. Inter.*, *151*, 206–222, doi:10.1016/j.pepi.2005.03.003.

Long, M. D., X. Xiao, Z. Jiang, B. Evans, and S.-i. Karato (2006), Lattice preferred orientation in deformed polycrystalline (Mg, Fe)O and implications for seismic anisotropy in D″, *Phys. Earth Planet. Inter.*, *156*, 75–88, doi:10.1016/j.pepi.2006.02.006.

Madi, K., S. Forest, P. Cordier, and M. Boussuge (2005), Numerical study of creep in two-phase aggregates with a large viscosity contrast: Implications for the rheology of the lower mantle. *Earth Planet. Sci. Lett.*, *237*, 223–238, doi:10.1016/j.epsl.2005.06.027.

Mao, W. L., Y. Meng, and H.-K. Mao (2010), Elastic anisotropy of ferromagnesian post-perovskite in Earth's D″ layer,

Phys. Earth Planet. Inter., *180*, 203–208, doi:10.1016/j.pepi.2009.10.013.

Marquardt, H., S. Speziale, H. J. Reichmann, D. J. Frost, F. R. Schilling, and E. J. Garnero (2009), Elastic shear anisotropy of ferropericlase in Earth's lower mantle, *Science*, *324*, 224–226, doi:10.1126/science.1169365.

McNamara, A. K., E. J. Garnero, and S. Rost (2010), Tracking deep mantle reservoirs with ultra-low velocity zones. *Sci. Lett.*, *299*, 1–9, doi:10.1016/j.epsl.2010.07.042.

Meade, C., P. G. Silver, and S. Kaneshima (1995), Laboratory and seismological observations of lower mantle isotropy, *Geophys. Res. Lett.*, *22*, 1293–1296, doi:10.1029/95GL01091.

Menke, W., and V. Levin (2003), The cross-convolution method for interpreting SKS splitting observations, with application to one and two-layer anisotropic earth models, *Geophys. J. Int.*, *154*, 379–392, doi:10.1046/j.1365-246X.2003.01937.x.

Merkel, S., A. K. McNamara, A. Kubo, S. Speziale, L. Miyagi, Y. Meng, T. S. Duffy, and H.-R. Wenk (2007), Deformation of (Mg,Fe)SiO$_3$ post-perovskite and D″ anisotropy, *Science*, *316*(5832), 1729–1732, doi:10.1126/science.1140609.

Miyagi, L., W. Kanitpanyacharoen, P. Kaercher, K. K. M. Lee, and H.-R. Wenk (2010), Slip systems in MgSiO$_3$ post-perovskite: Implications for D″anisotropy, *Science*, *329*, 1639–1641, doi:10.1126/science.1192465.

Murakami, M., K. Hirose, K. Kawamura, N. Sata, and Y. Ohishi (2004), Post-perovskite phase transition in MgSiO$_3$, *Science*, *304*, 855–858, doi:10.1126/science.1095932.

Niu, F., and A. M. Perez (2004), Seismic anisotropy in the lower mantle: A comparison of waveform splitting of SKS and SKKS, *Geophys. Res. Lett.*, *31*, L24612, doi:10.1029/2004GL021196.

Nowacki, A., J. Wookey, and J.-M. Kendall (2010), Deformation of the lowermost mantle from seismic anisotropy, *Nature*, *467*, 1091–1094, doi:10.1038/nature09507.

Oganov, A., R. Martonak, A. Laio, P. Raiteri, and M. Parrinello (2005), Anisotropy of Earth's D″ layer and stacking faults in the MgSiO$_3$ post-perovskite phase, *Nature*, *438*(7071), 1142–1144, doi:10.1038/nature04439.

Panning, M., and B. Romanowicz (2004), Inferences on flow at the base of Earth's mantle based on seismic anisotropy, *Science*, *303*(5656), 351–353, doi:10.1126/science.1091524.

Restivo, A., and G. Helffrich (2006), Core–mantle boundary structure investigated using SKS and SKKS polarization anomalies, *Geophys. J. Int.*, *165*, 288–302, doi:10.1111/j.1365-246X.2006.02901.x.

Rokosky, J., T. Lay, E. Garnero, and S. Russell (2004), High-resolution investigation of shear-wave anisotropy in D″ beneath the Cocos Plate, *Geophys. Res. Lett.*, *31*, L07605, doi:10.1029/2003GL018902.

Silver, P. G., and W. W. Chan (1991), Shear-wave splitting and subcontinental mantle deformation, *J. Geophys. Res.*, *96*, 16,429–16,454, doi:10.1029/91JB00899.

Stackhouse, S., J. P. Brodholt, J. Wookey, J. M. Kendall, and G. D. Price (2005), The effect of temperature on the seismic anisotropy of the perovskite and post-perovskite polymorphs of MgSiO$_3$, *Earth Planet. Sci. Lett.*, *230*, 1–10, doi:10.1016/j.epsl.2004.11.021.

Stixrude, L. (1998), Elastic constants and anisotropy of MgSiO$_3$ perovskite, periclase and SiO$_2$ at high pressure, in *The Core-Mantle Boundary Region*, *Geodyn. Ser.*, vol. 28, edited by M. Gurnis et al., pp. 83–96, AGU, Washington, D. C.

Thomas, C., and J. M. Kendall (2002), The lowermost mantle beneath northern Asia—II. Evidence for lower-mantle anisotropy, *Geophys. J. Int.*, *151*, 296–308, doi:10.1046/j.1365-246X.2002.01760.x.

Thorne, M. S., and E. J. Garnero (2004), Inferences on ultra-low-velocity zone structure from a global analysis of SPdKS waves, *J. Geophys. Res.*, *109*, B08301, doi:10.1029/2004JB003010.

Tono, Y., Y. Fukao, T. Kunugi, and S. Tsuboi (2009), Seismic anisotropy of the Pacific slab and mantle wedge beneath the Japanese islands, *J. Geophys. Res.*, *114*, B07307, doi:10.1029/2009JB006290.

Trampert, J., F. Deschamps, J. Resovsky, and D. Yuen (2004), Probabilistic tomography maps chemical heterogeneities throughout the lower mantle, *Science*, *306*, 853–856, doi:10.1126/science.1101996.

Tsuchiya, T., J. Tsuchiya, K. Umemoto, and R. M. Wentzcovitch (2004), Phase transition in MgSiO$_3$ perovskite in the Earth's lower mantle, *Earth Planet. Sci. Lett.*, *224*, 241–248, doi:10.1016/j.epsl.2004.05.017.

Usui, Y., Y. Hiramatsu, M. Furumoto, and M. Kanao (2005), Thick and anisotropic D″ layer beneath Antarctic Ocean, *Geophys. Res. Lett.*, *32*, L13311, doi:10.1029/2005GL022622.

van der Hilst, R. D., M. V. de Hoop, P. Wang, S.-H. Shim, P. Ma, and L. Tenorio (2007), Seismostratigraphy and thermal structure of Earth's core-mantle boundary region, *Science*, *315*, 1813–1817, doi:10.1126/science.1137867.

van der Meer, D. G., W. Spakman, D. J. J. van Hinsbergen, M. L. Amaru, and T. H. Torsvik (2010), Towards absolute plate motions constrained by lower-mantle slab remnants, *Nat. Geosci.*, *3*, 36–40, doi:10.1038/ngeo708.

Vinnik, L. P., R. Kind, G. L. Kosarev, and L. Makeyeva (1989), Azimuthal anisotropy in the lithosphere from observations of long-period S-waves, *Geophys. J. Int.*, *99*, 549–559, doi:10.1111/j.1365-246X.1989.tb02039.x.

Visser, K., J. Trampert, and B. L. N. Kennett (2008), Global anistropic phase velocity maps for higher mode Love and Rayleigh waves, *Geophys. J. Int.*, *172*, 1016–1032, doi:10.1111/j.1365-246X.2007.03685.x.

Walker, A. M., A. M. Forte, J. Wookey, A. Nowacki, and J.-M. Kendall (2011), Elastic anisotropy of D″ predicted from global models of mantle flow, *Geochem. Geophys. Geosyst.*, *12*, Q10006, doi:10.1029/2011GC003732.

Wang, Y., and L. Wen (2007), Complex seismic anisotropy at the border of a very low velocity province at the base of the Earth's mantle, *J. Geophys. Res.*, *112*, B09305, doi:10.1029/2006JB004719.

Wenk, H.-R., S. Cottaar, C. T. Tome, B. Romanowicz, and A. K. McNamara (2011), Deformation in the lowermost mantle: From polycrystal plasticity to seismic anisotropy, *Earth Planet. Sci. Lett.*, *306*, 33–45, doi:10.1016/j.epsl.2011.03.021.

Wentzcovitch, R. M., T. Tsuchiya, and J. Tsuchiya (2006), MgSiO$_3$ postperovskite at D″ conditions, *Proc. Natl. Acad. Sci. U. S. A.*, *103*, 543–546, doi:10.1073/pnas.0506879103.

Wessel, P., and W. H. F. Smith (1995), New version of the generic mapping tool released, *Eos Trans. AGU*, *76*(33), 329, doi:10.1029/95EO00198.

Wirth, E., and M. D. Long (2010), Frequency-dependent shear wave splitting beneath the Japan and Izu-Bonin subduction zones, *Phys. Earth Planet. Inter.*, *181*, 141–154, doi:10.1016/j.pepi.2010.05.006.

Wookey, J., and J. M. Kendall (2004), Evidence of mid-mantle anisotropy from shear wave splitting and the influence of

shear-coupled P waves, *J. Geophys. Res.*, *109*, B07309, doi:10.1029/2003JB002871.

Wookey, J., and J. M. Kendall (2007), Seismic anisotropy of post-perovskite and the lowermost mantle, in *Post-Perovskite: The Last Mantle Phase Transition*, *Geophys. Monogr. Ser.*, vol. 174, edited by K. Hirose et al., pp. 171–189, AGU, Washington, D. C.

Wookey, J., and J. M. Kendall (2008), Constraints on lower-most mantle mineralogy and fabric beneath Siberia from seismic anisotropy, *Earth Planet. Sci. Lett.*, *275*, 32–42, doi:10.1016/j.epsl.2008.07.049.

Wookey, J., J. M. Kendall, and G. Rümpker (2005), Lower-most mantle anisotropy beneath the north Pacific from differential S–ScS splitting, *Geophys. J. Int.*, *161*, 829–838, doi:10.1111/j.1365-246X.2005.02623.x.

Wüstefeld, A., and G. Bokelmann (2007), Null detection in shear-wave splitting measurements, *Bull. Seismol. Soc. Am.*, *97*, 1204–1211, doi:10.1785/0120060190.

Wüstefeld, A., G. Bokelmann, G. Barruol, and C. Zaroli (2008), Splitlab: A shear-wave splitting environment in Matlab, *Comput. Geosci.*, *34*, 515–528, doi:10.1016/j.cageo.2007.08.002.

Wysession, M. E., T. Lay, J. Revenaugh, Q. Williams, E. J. Garnero, R. Jeanloz, and L. H. Kellogg (1998), The D″ discontinuity and its implications, in *The Core-Mantle Boundary Region*, *Geodyn. Ser.*, vol. 28, edited by M. Gurnis et al., pp. 273–297, AGU, Washington, D. C.

Yamazaki, D., and S. Karato (2002), Fabric development in (Mg,Fe)O during large strain, shear deformation; implications for seismic anisotropy in Earth's lower mantle, *Phys. Earth Planet. Inter.*, *131*, 251–267, doi:10.1016/S0031-9201(02)00037-7.

Yamazaki, D., T. Yoshino, H. Ohfuji, J. i. Ando, and A. Yoneda (2006), Origin of seismic anisotropy in the D″ layer inferred from shear deformation experiments on post-perovskite phase, *Earth Planet. Sci. Lett.*, *252*, 372–378, doi:10.1016/j.epsl.2006.10.004.